Revista Mexicana de Física
ISSN: 0035-001X
rmf@ciencias.unam.mx
Sociedad Mexicana de Física A.C.
México

Carvajal, E.; Hahn-Herrera, O.; Orgaz, E.
Density functional investigation of silver, palladium and silver-palladium small sized clusters
Revista Mexicana de Física, vol. 55, núm. 6, diciembre, 2009, pp. 418-424
Sociedad Mexicana de Física A.C.
Distrito Federal, México

Density functional investigation of silver, palladium and silver-palladium small sized clusters

E. Carvajal[a], O. Hahn-Herrera[a], and E. Orgaz[a,b]

[a]*Departamento de Física y Química Teórica, Facultad de Química, Universidad Nacional Autónoma de México, 04510, México, D.F. México.*

[b]*Departamento de Química, Centro de Investigación y de Estudios Avanzados del Instituto Politécnico Nacional, Avenida Politécnico Nacional 2508, Apartado Postal 14740, 07000, México, D.F., México.*

Recibido el 21 de enero de 2009; aceptado el 5 de noviembre de 2009

We have investigated the geometrical and electronic properties of small sized Ag and Pd as well as bimetallic Ag-Pd clusters. By means of a pseudopotential scheme within density functional theory, we found the ground-state geometries and the spin multiplicity state for this family of metallic clusters. We computed the binding energy and the atom addition energy change for these family of clusters with two different density functionals. Ag and Pd cluster series exhibit a clear different behavior as a consequence of the atomic electronic structure. In particular we discuss the high symmetry silver clusters and the trends in the small sized bimetallic Ag-Pd systems.

Keywords: Silver; palladium and silver-palladium clusters; electronic structure.

En este trabajo presentamos los resultados del estudio de la propiedades estructurales y electrónicas de cúmulos pequeños de Ag y Pd así como cúmulo bimetálicos Ag-Pd. Haciendo uso de pseudopotenciales en un esquema basado en teoría de los funcionales de la densidad electrónica, determinamos las propiedades geométricas la multiplicidad de espín del estado fundamental para estos sistemas. Calculamos la energías de cohesión y la energía de adición de átomos para estas familias de cúmulos haciendo uso de dos distintos funcionales de la densidad. Las dos series de cúmulos de Ag y Pd muestran claramente comportamientos distintos.En particular, discutimos los resultados de cúmulos de alta simetría y las tendencias en loas cúmulos bimetálicos Ag-Pd

Descriptores: Plata; cúmulo de paladio y plata-paladio; estructura electrónica.

PACS: 73.22.-f 61.46.Bc 75.75.+a

1. Introduction

In recent years there has been a growing interest in the applications of hydrogen in fuel cells for energy consumption. In particular, the production of hydrogen has been traditionally associated with the reforming of hydrocarbons. Scientific as well as technological efforts are underway to overcome this paradoxical situation. As an alternative method of hydrogen production, the ethanol steam reforming process are begin actively investigated [1]. Palladium and palladium alloys exhibit a strong affinity for hydrogen, acting as catalyst in this kind of process. Palladium is an expensive metal and the interest in alloying it to reduce the cost as well as to increase the performance is of great interest. However, palladium rich Pd-Ag alloys tend to exhibit surface segregation when exposed to a H_2 atmosphere. Surfaces of the Pd_3Ag intermetallic and related alloys have been investigated in recent years from both experimental and theoretical viewpoints [1–3]. Surface supported Ag-Pd clusters are interesting in order to design new catalyst. This possibility has been recently considered by Wang *et al*. [4] in the case of Pd clusters supported over MgO and adsorbed organic molecules in small Pd clusters [5], supported on γ-Al_2O_3.

In this contribution we investigated the stability and electronic properties of small-sized silver, palladium and silver-palladium clusters. In the following section we outline the methodological aspects. Our results on the small-sized Ag_n, Pd_m and Pd_mAg_n clusters are presented and discussed.

2. Methodology

The $Ag_n(Pd_m)$ clusters were investigated up to n=14 (m=9) and Pd_mAg_n up to m+n=5. Computations of the electronic structure were performed within the density functional theory (DFT) as coded in the Gaussian package [6]. We employed the non-relativistic pseudopotential electron core potentials and basis set LANL2DZ [7]. The number of active (extended valence) electrons is 18 (19) for Pd (Ag). The exchange and correlation potential was introduced by selecting a suitable density functional. In this research we employed two different generalized gradient approximated (GGA) functionals, PW91 [8] and PBE [9]. We have also considered the B3LYP hybrid functional since it has been shown that these kinds of density functionals can yield reliable energetics and structural results for silver and copper compounds [10–13]. Full geometry optimization was carried out, without symmetry constraints, for all Ag, Pd and Pd-Ag clusters. We verified systematically that a stable geometry was obtained by computing and inspecting the hessian matrix and testing different electron spin multiplicities. For the metallic clusters under study, the initial geometries were selected by a Genetic Algorithm [14] method employing the so-called Gupta potential [15] (GAGP). This technique, as well as many others, [14] does not necessarily predict the ground state structure. However, this is a good enough starting point provided that the symmetry constraints in a high symmetry cluster are properly relaxed. Otherwise, a local minimum can

be found that does not correspond to the ground-state structure. For each starting geometry, we tested different allowed spin multiplicities in order to guarantee that we found the ground state structure. In addition, the starting geometry for each cluster has been compared with previous investigations, when available. We energetically characterized each cluster by computing the binding energy (BE) accordingly to the decomposition reaction $M_n \longrightarrow$ nM: BE=nE(M)-E(M_n), where E(M_n) is the total electronic energy for the cluster containing n metallic atoms. The atom addition energy change [$\Delta E_1(M_n)$] has been computed. These values correspond to the cluster growing reaction M_{n-1} + M $\longrightarrow$ M_n. The corresponding energy balance is:

$$\Delta E_1(M_n) = E(M_n) - E(M_{n-1}) - E(M).$$

If the M_n cluster is more stable than the preceding n-1 structure, we expect a large gain (negative) change respect to M_{n-1} and a free M atom. These values are used to compute the very common *second energy difference* which is usually defined by

$$\begin{aligned}\Delta E_2(M_n) &= E(M_{n+1}) + E(M_{n-1}) - 2E(M_n) \\ &= \Delta E_1(M_{n+1}) - \Delta E_1(M_n).\end{aligned}$$

3. Results and discussion

3.1. Silver clusters

We have explored the more stable structures for Ag_n clusters and we found that the ground-state structures (sketched in Fig. 1) are consistent with those previously obtained [16–24], being planar up to n=6. The first three-dimensional silver cluster is Ag_7 exhibiting a pentagonal bi-pyramid structure. It should be indicated that the spin multiplicity of the ground-state clusters is consistent with those recently published by Pereiro *et al.* [20]. However, our results of the geometry optimization for the Ag_{13} cluster yield a low symmetry structure in a doublet ground-state. This structure appears to be 1.17eV/Ag_{13} (PBE computations) more stable than the icosahedral cluster. This result is in contradiction with the icosahedral structure proposed by Pereiro *et al.* [20] and consistent with the Jahn-Teller distorted icosahedron claimed by Zhao *et al.* [16] and the low symmetry structure found by Fernández *et al.* [25], Chang *et al.* [27] and Sun *et al.* [26]. Computations of the electronic structure of 4d transition metals in several high and low symmetry structures [27] indicate that a low symmetry form (C_{2v}) is systematically more stable than the high symmetry (I_h and fcc-derived) structures, for the late transition metals (Tc-Cd). The most important consequence of this symmetry reduction is the breaking of the electron state degeneracy and the reduction of the cluster's magnetic moment. In the icosahedral Ag_{13} cluster the HOMO level is composed by a doubly degenerate α-state and a triply degenerate β-state at 0.16 eV below (Fig. 2). These states are occupied with five unpaired electrons conferring to this cluster the high magnetic moment found by Pereiro *et al.* [20] and Reddy *et al.* [28]. However, the HOMO in the ground state structure is a singly degenerate state occupied by one unpaired electron. The HOMO-LUMO gap in the stable (icosahedral) structure is 0.71 eV (0.60eV), while the HOMO to HOMO-1 energy distance is 0.68 eV (2.23eV). The case of the Ag_{14} is similar: we found a singlet non-symmetrical structure for the ground-state. This result is in opposition to the derived icosahedral (C_{3v}) quintet structure found by Pereiro *et al.* [20]. Our proposal is 1.06 eV/Ag_{14} more stable.

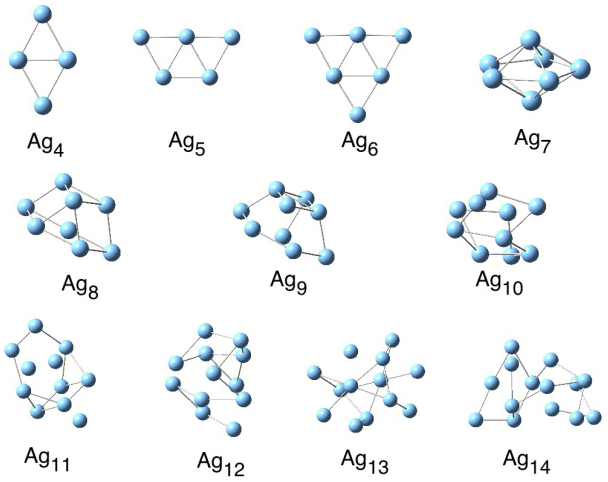

FIGURE 1. Schemes of the more stable geometries for the Ag_n clusters (n=4 to 14). The ground state multiplicities are singlets for clusters with even number of atoms and doublet for the clusters with odd number of atoms.

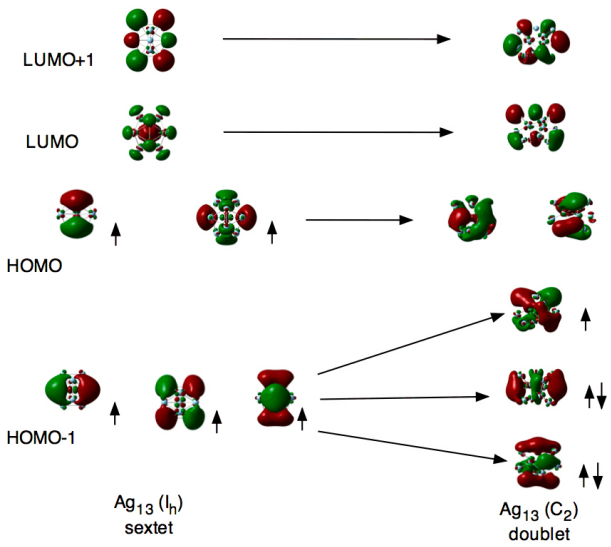

FIGURE 2. Schematic molecular orbital diagram for Ag_{13} in the stable sextet icosahedral (I_h) symmetry and in the stable doublet C_{2v} symmetry.

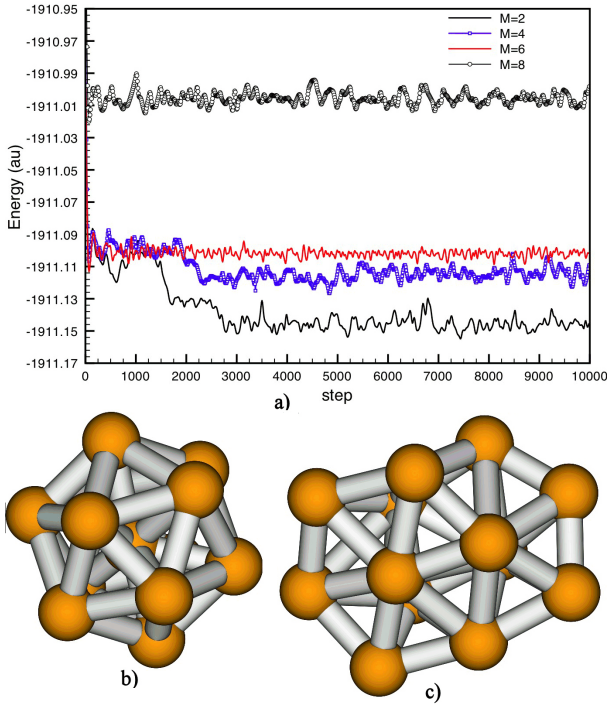

FIGURE 3. (a) Energy path for the Born-Oppenheimer Molecular Dynamics simulation of Ag_{13} at different multiplicities (M). The time step where set to 1 fs. Geometry of the Ag_{13} cluster obtained in the sextet state and (c) in the doublet state.

In order to complete the view of the Ag_{13} cluster stability, we have carried out a Born-Oppenheimer molecular dynamics simulation [29] during a long time scale. We considered different multiplicities going from the doublet to octet state. In Fig. 3a we plot the energy change along the time. The first steps correspond to the icosahedral Ag_{13} structure that we selected as the starting point as suggested by the GAGP technique. We observed that for the sextet and octet multiplicities, the preferred structure remain the icosahedral one (Fig. 3b). It is interesting to note that for the sextet case, the energy window along the time remains small, indicating the small fluctuations around the stable geometry. However, in particular for low multiplicities, these energy windows appreciably increase indicating now the large fluctuations around the stable fcc-like structure (Fig. 3c). It is remarkable that the structure sketched in Fig. 3c corresponds to that obtained in the ab initio local optimization (Fig. 1). Since all the computations were carried out at the same theory level, the energy scale indicates also the relative stability of the clusters. Thus, the doublet structure is clearly more stable than the others. We do not observe the energy path crossing in Fig. 3a, which should tell us that a possible change in multiplicity should be considered.

In Fig. 4a we plot the computed binding energy for the Ag_n series. As can be appreciated, the obtained results exhibit an excellent consistency regardless of the GGA density functional employed. Moreover, the cases of Ag_{13}, and Ag_{14} do not exhibit any particular anomaly: their binding energy

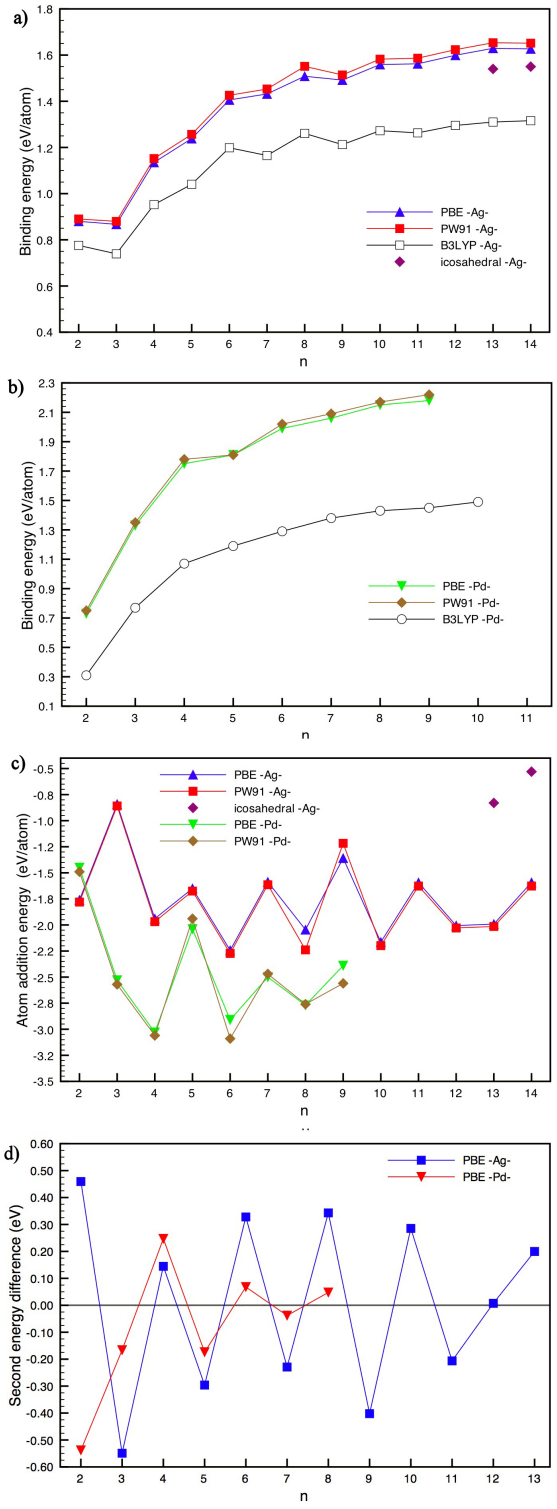

FIGURE 4. (a) Binding energy (eV/atom) along the Ag_n series. (b) Binding energy (eV/atom) along the Pd_m series. (c) Atom addition energy E (eV/atom) along the Ag_n and Pd_m series. (d) Second energy difference (eV) for the Ag_n and Pd_m series. The symbols labelled *icosahedral* correspond to the icosahedral Ag_{13} and icosahedral-derived Ag_{14} clusters.

values are in line with the general trend. In this plot we included the binding energies obtained for the icosahedral Ag_{13} and icosahedral-derived Ag_{14} clusters computed with the PBE density functional. The computed values of the binding energy are, as expected, smaller than those found for the ground-state structures and clearly out of the general trend. In Fig. 4c-d we plot the energy change associated with the addition of an Ag atom and the second energy difference as previously defined. In these figures we clearly observe that the even electron number clusters exhibit a larger gain in energy than the odd electron structures.

It must be noted that our results for the binding energies using the B3LYP hybrid density functional are underestimated with respect to the GGA results. In addition B3LYP computations exhibit important structural differences with respect to the GGA results. This behavior is in agreement with the recent results of Zhao *et al.* [13] on small silver clusters.

3.2. Palladium clusters

We investigated Pd_m clusters up to m=9. In Fig. 5 we sketch the ground-state structures indicating the corresponding spin multiplicity. The binding energy for the Pd series as well as the addition energy and second energy difference are plotted in Figures 4b-d. Once again, the consistency of the computations is remarkable regardless the GGA density functional employed. However, the B3LYP density functional does not perform in a correct manner for the energetic nor for structural aspects. Pd_3 and Pd_4 exhibit triangular and tetrahedral structures in a triplet state. This is in agreement with several previous computations carried out at different theory levels; extended Hückel [30, 31], and DFT techniques using pseudopotentials [27,32–34] and relativistic electron core potentials [35]. Genetic algorithms have been used along with ab initio techniques to find the ground-state of Pd_m clusters [37]. However, only the high symmetry structures were found which it is now clear that they are not the more stable ones [27, 32]. The case of the high symmetry structures of Pd_{13} is symptomatic of this complexity [38]. However, Yacamán *et al.* [39] have experimentally found Pd_m clusters up to 5nm, having high symmetry forms. We face, in the case of palladium clusters, the same problems previously discussed for silver systems. After our computations, Pd_5 exhibit a triangular bi-pyramid (close to D_{3h} symmetry) structure in a triplet state. This finding is in excellent agreement with the results of extensive computations within relativistic electron core potentials in a CASSCF scheme for several Pd_5 structures carried out by Dai and Balasubramanian [36]. Recently, Zhang *et al.* [40] have investigated middle sized Pd_m

TABLE I. Relative energy (eV) for the Pd clusters at different multiplicities (M), computed at PBE level of theory.

	M =1	M =3	M =5
Pd_2	0.19	0.00	1.12
Pd_3	0.05	0.00	0.74
Pd_4	0.11	0.00	0.41
Pd_5	0.00	0.29	0.14
Pd_6	0.07	0.00	0.08
Pd_7	0.01	0.00	0.02
Pd_8	0.02	0.00	0.01
Pd_9	0.00	0.00	0.01

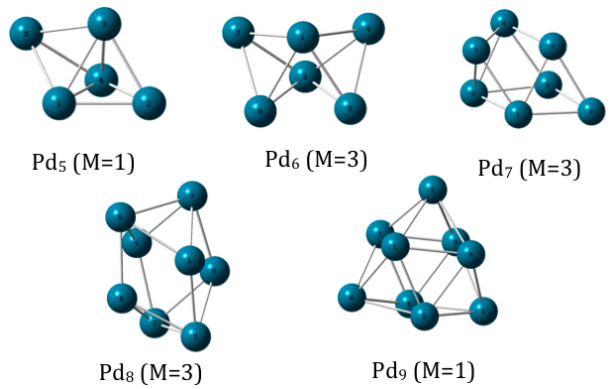

FIGURE 5. Schemes of the more stable geometries for the Pd_m clusters. The multiplicity of the ground-state is indicated.

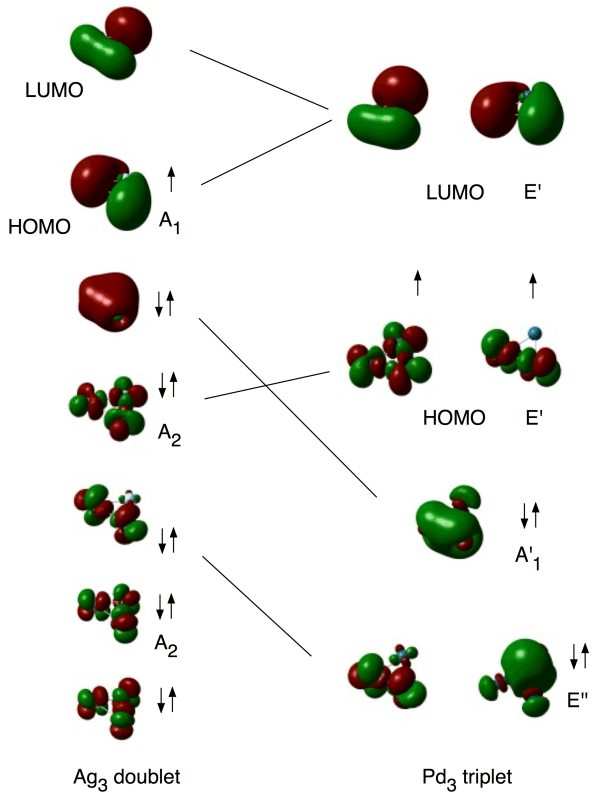

FIGURE 6. Schematic molecular orbital diagram for the stable doublet Ag_3 (C_{2v}) and triplet Pd_3 (D_{3h}) clusters.

TABLE II. Relative energy ΔE (eV) for the Ag_n and Pd_m clusters at different multiplicities (M), computed at PBE level of theory. The integer number preceding the energy value indicates the spin multiplicity

Ag:Pd	M/ΔE	M/ΔE	M/ΔE
1:1	2 / 0.00	4 / 0.08	6 / 0.28
2:1	1 / 0.00	3 / 0.05	5 / 0.15
1:2	2 / 0.00	4 / 0.07	6 / 0.15
2:2	1 / 0.00	3 / 0.03	5 / 0.11
1:3	2 / 0.00	4 / 0.06	6 / 0.13
3:1	2 / 0.00	4 / 0.08	6 / 0.18
1:4	2 / 0.00	4 / 0.03	6 / 0.08
2:3	1 / 0.00	3 / 0.03	5 / 0.07
3:2	2 / 0.00	4 / 0.05	6 / 0.11
4:1	1 / 0.00	3 / 0.02	5 / 0.10

TABLE III. Data for the Ag_nPd_m (n+m=3) clusters. Multiplicity of the ground-state (M), shortest metal-metal distance (d in Å), largest bond angle (θ), binding energy (BE in eV) computed at PBE level of theory.

	Ag_3	Ag_2Pd	$AgPd_2$	Pd_3
M	doublet	singlet	doublet	triplet
d	2.66	2.64	2.66	2.54
θ	71.5	62.4	56.6	60.6
BE	0.87	1.24	1.29	1.33
point group	C_{2v}	C_{2v}	C_{2v}	D_{3h}

(m=15-25) clusters. It is now clear that the different possible ground-state geometries differ by a small amount of energy which will become irrelevant when these nanostructures interact with, for example, surfaces or molecules. Moreover, the transition states as well as the size of the energy barriers connecting different stable structures are in general unknown.

3.3. Silver-palladium clusters

Ag clusters adopt tridimensional structures for n≥7 whereas Pd clusters do so when m≥4. This is understandable since Ag is a noble metal having filled d-shell ($4d^{10}5s^1$) and exhibiting essentially σ interactions through the 5s orbitals. Pd atoms exhibit an atomic electronic configuration between $4d^{10}5s^0$ and $4d^95s^1$. This opens the possibility of d-electron interactions. In what follows we will compare the bonding details in the simplest clusters: Ag_3 and Pd_3 . This analysis will be helpful in discussing the more complex bonding situation in the Ag-Pd clusters. We selected Ag_3 and Pd_3 since both stable structures are obviously planes and the coordination effects that could arise in more complex clusters are absent. The Pd_3 cluster exhibits Pd-Pd distances of 2.54 Å and a bond angle close to 60°. This means that the point symmetry of this cluster is close to D_{3h}. Owing to the closeness to the D_{3h}

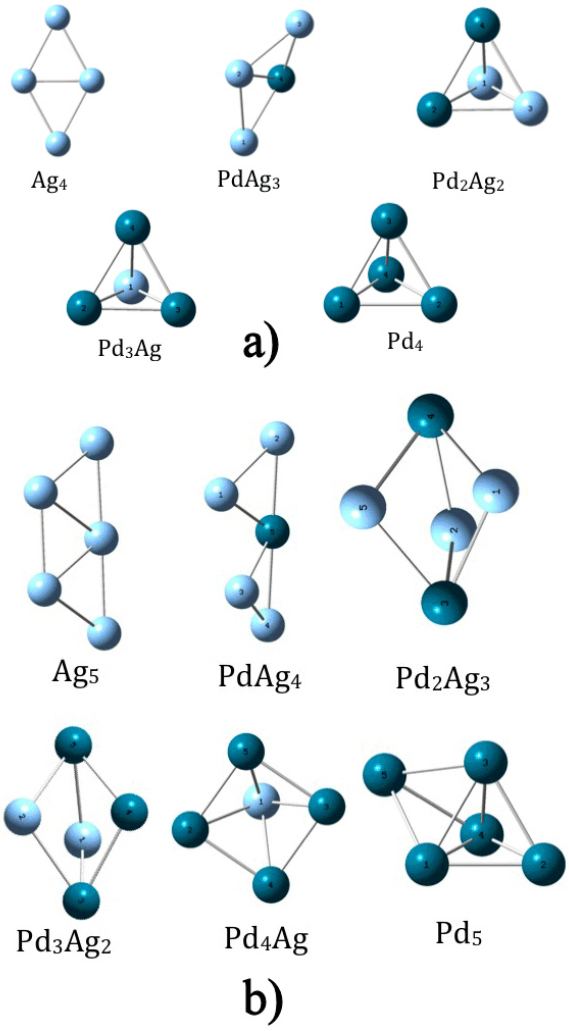

FIGURE 7. Schemes of the more stable geometries for the (a) Ag_nPd_{4-n} clusters and (b) for the Ag_nPd_{5-n} clusters. The multiplicity of the ground-state is indicated.

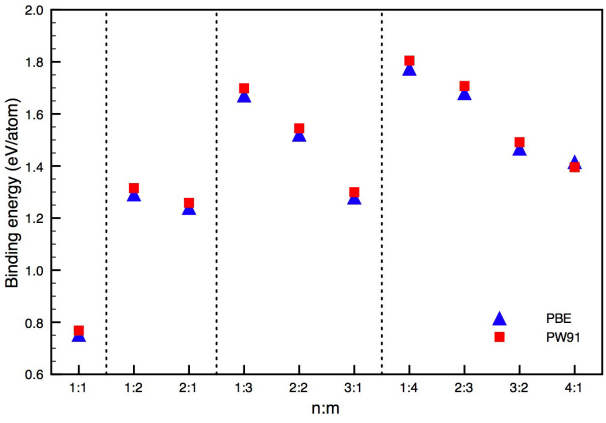

FIGURE 8. Binding energy (eV/atom) along the Pd_mAg_n series computed with two different density functionals: $Pd_mAg_n \longrightarrow$ nAg + mPd.

symmetry, the cluster exhibits accidental degeneracies in particular at the HOMO level, stabilizing the Pd_3 system in a triplet state, 0.15 eV below the singlet one (see Fig. 6). The quintet structure is clearly less favorable, exhibiting a total energy 2.22 eV above the ground state. The case of the Ag_3 system is very clear: the Ag-Ag bond distance is 2.66Å and the largest bond angle is 71.5°. Now the C_{2v} symmetry is stable and the system, having three more electrons than the Pd analogue, exhibits a doublet ground-state. The inspection of the molecular orbitals energy diagram (Fig. 6) clearly exhibits the role of the d states in the bonding of Pd_3. For Pd_m where m $\geq$ 4, the tridimensional structures are easily stabilized. The binding energy for the Pd trimer is clearly larger than for the Ag series. This trend is maintained until the tridimensional structures appears in Ag_n clusters. However, the Pd clusters are systematically more tightly bound than the Ag ones. The results for the $Ag_{3-m}Pd_m$ clusters show that the preferred symmetry is C_{2v}, excepting the Pd_3 case (Table II). The Pd-Ag distance is essentially constant for Ag_2Pd and $AgPd_2$, while an important reduction in the metal-metal distance occurs for Pd_3. The largest bonding angle is observed for Ag_3, indicating the small tendency to form three-dimensional structures. This is in line with the small computed binding energy (0.87eV). The bonding angle for $AgPd_2$ is smaller than 60° since the Pd-Pd interaction dominates. This is indicative of the tendency of Pd to form three-dimensional structures, which is also evident in the binding energy which increases up to 1.33 eV for Pd_3.

These observations are strongly reinforced in the series of bimetallic clusters $Ag_{4-m}Pd_m$ and $Ag_{5-m}Pd_m$. The ground-states structures are sketched in Figs. 7. In all the computed systems, the ground-state spin multiplicity corresponds to the lowest admitted by the bimetallic cluster. We observe again the strong tendency of palladium to create three-dimensional structures. While Ag_4 and Ag_5 are both planar, the first Pd substitution introduces a breaking on the cluster planarity. In these series, the clusters with two Pd atoms exhibit geometries very close to the complete substituted system: Pd_4 and Pd_5. In Fig. 8 we plotted the binding energy for the bimetallic cluster series and in Table III a résumé of the relative energies for different multiplicities is listed . It is worth noting that the binding energy seems to obey a simple mixing rule: the binding energy diminishes linearly when the Ag content increases. This is perhaps an announcement of the bulk phase diagram for Ag-Pd, a solid solution for all the composition range.

4. Conclusions

We have investigated the geometrical and electronic properties of small-sized Ag_n and Pd_m as well as bimetallic Ag_nPd_m clusters. By means of a pseudopotential scheme within the density functional theory, we found the ground-state geometries and spin multiplicities for this family of metallic clusters. We computed the binding energy and the atom addition energy change for these family of clusters with two different density functionals. We found that this property increases smoothly when the number of atoms in the cluster increases. We confirm the low symmetry (low spin) ground-state of Ag_{13} and Ag_{14} exhibiting a total energy higher than the high symmetry structures. In addition, the high symmetry structures do not exhibit the general trend observed by the remaining silver clusters. The palladium cluster series exhibit a different behavior from the Ag series. Two aspects retain our attention the tendency to form three-dimensional structures and the significant increase of the binding energy compared to the corresponding silver clusters. We explain this behavior by considering the role of the 4d valence electrons, which are clearly active in the Pd-Pd chemical bonding. Moreover, the Pd-4d states are a dominant factor in the behavior of the bimetallic Ag_nPd_m clusters. The bimetallic series seems to follow a linear (simple) mixing rule as the binding energy trend suggests. We found this of special interest since the bulk Ag-Pd phase diagram exhibits a solid solution along the complete composition range.

Acknowledgments

Financial support was provided by DGAPA-UNAM under grant number IN101106. We wish to thank the DGSCA-UNAM for granting us access to their supercomputing facility. E.C. would like to thank the DGAPA-UNAM for the PROFIP postdoctoral fellowship.

1. W.-H. Lin, C.-S. Hsiao, and H.-F. Chang, *J. Membrane Science* **322** (2008) 360.
2. N. Ozawa, N.B. Arboleda Jr., H. Nakanishi, and H. Kasai, *Surface Science* **602** (2008) 859
3. O.M. Lovvik and S. Opalka, *Surface Science* **602** (2008) 2840.
4. Y. Wang and T.N. Truong, in press *J. Phys. Chem. C* **112** (2008) 13674.
5. J.W. de M. Carneiro and M.T. de M. Cruz, in press *J. Phys. Chem. A* **112** (2008) 8929.
6. Gaussian 03, Revision C.02, M.J. Frisch, *et al*. Gaussian, Inc., (Wallingford CT, 2004).
7. P.J. Hay and W.R. Wadt, *J. Chem. Phys.* **82** (1985) 299.
8. J.P. Perdew, K. Burke, and Y. Wang, *Phys. Rev. B* **54** (1996) 16533.
9. J.P. Perdew, K. Burke, and M. Ernzerhof, *Phys. Rev. Lett.* **78** (1997) 1396.
10. A. Ramírez-Solís, R. Poteau, A. Vela, and J.P. Daudey, *J. Chem. Phys.* **122** (2005) 164306.

11. A. Ramírez-Solís, R. Poteau, and J.P. Daudey, *J. Chem. Phys.* **124** (2006) 034307.
12. A. Ramírez-Solís, *J. Chem. Phys.* **126** (2007) 224105.
13. S. Zhao *et al.*, *J. Chem. Phys.* **124** (2006) 184102.
14. R. Ferrando, J. Jellinek, and R.L. Johnstons, *Chem. Rev.* **108** (2008) 845
15. R.P. Gupta, *Phys. Rev. B* **23** (1981) 6265.
16. J. Zhao, Y. Luo, and G. Wang, *Eur. Phys. J. D* **14** (2001) 309
17. M.N. Huda and A.K. Ray, *Phys. Rev. A* **67** (2003) 013201.
18. Y. Wang and X.G. Gong, *Eur. Phys. J.D*, **34** (2005) 19.
19. M. Pereiro and D. Baldomir, *Phys. Rev. A* **75** (2007) 033202.
20. M. Pereiro, D. Baldomir, and J.E. Arias, *Phys. Rev. A* **75** (2007) 063204.
21. T.L. Haslett, K.A. Bosnick, and M. Moskovits, *J. Chem. Phys.* **108** (1998) 3453
22. D. Alamanova, V.G. Grigoryan, and M. Springborg, *J. Phys. Chem C.* **111** (2007) 12577
23. Y.-P. Chiu, Ch.-M. Wei, and C.-S. Chang, *Phys. Rev. B* **78** (2008) 115402.
24. M. Yang, K.A. Jackson, and J. Jellinek, *J. Chem. Phys.* **125** (2006) 144308.
25. E.M. Fernández, J.M. Soler, I.L. Garzón, and L.C. Balbás, *Phys Rev B* **70** (2004) 165403.
26. Y. Sun, M. Zhang, and R. Fournier, *Phys. Rev. B* **77** (2008) 075435.
27. C.M. Chang and M.Y. Chou, *Phys. Rev. Lett.* **93** (2004) 133401.
28. B.V. Reddy, S.N. Khanna, and B.I. Dunlap, *Phys. Rev. Lett.* **70** (1993) 3323.
29. BOMD computations were carried out with the deMon2k code. A.M. Köster *et al.*, The deMon developers, Cinvestav, Mexico City, 2006. Nosé bath, NVT ensemble at 300K. The simulation time step was set to 1fs.
30. I. Efremenko and M. Sheintuch, *Surf. Sci.* **414** (1998) 148.
31. I. Efremenko and M. Sheintuch, *J. of Molecular Catalysis A: Chemical* **160** (2000) 445.
32. T. Futschek, M. Marsman, and J. Hafner, *J. Phys.: Condens. Matter* **17** (2005) 5927.
33. C. Luo *et al.*, *Int. J. Quantum Chem.* **107** (2007) 1632.
34. V. Kumar and Y. Kawazoe, *Phys. Rev. B* **66** (2002) 144413.
35. C. Xiao, S. Kruger, T. Belling, M. Mayer, and N. Rosch, *Int. J. Quantum Chem.* **74** (1999) 405.
36. D. Dai and K. Balasubramanian, *Chem. Phys. Lett.* **310** (1999) 303.
37. J. Rogan *et al.*, *Phys. Rev B* **72** (2005) 115421.
38. M. Moseler, H. Häkkinen, R.N. Barnett, and U. Landman, *Phys. Rev Lett.* **86** (2001) 2545.
39. M. José-Yacamán, M. Marín-Almazo, and J.A. Ascencio, *J. of Molecular Catalysis A: Chemical* **173** (2001) 61.
40. H. Zhang, D. Tian, and J. Zhao, *J. Chem. Phys.* **129** (2008) 114302l